Wireless sensor node demonstrating indoor-light energy harvesting and voltage-triggered duty cycling

M. A. Cowell[1], B. P. Lechene[1], P. Raffone[2], J. W. Evans[1], A. C. Arias[1], and P. K. Wright[1]

[1] Advanced Manufacturing for Energy, University of California, Berkeley CA 94720, USA
[2] Politecnico di Milano, Piazza Leonardo Da Vinci, Italy

E-mail: martin.cowell@berkeley.edu

Abstract. We demonstrate a wireless sensor node (WSN) that operates purely on harvested ambient indoor light energy and regulates its duty cycle via voltage-triggered sensing and transmission. The extremely low-power light found in indoor environments can be considered at first sight as unsuitable for high-power load demands characteristic of radios [1], but by leveraging spectrum-tailored solar cells, trickle charging a high-power energy reservoir, and implementing triggered duty cycling, we show that these power demands can be consistently met. All energy harvesting and storage components are fabricated in our labs.

1. Introduction

Indoor ambient light is a readily available source of energy for microelectronic devices, but its low power density has typically meant it is not considered for wireless snesor node (WSN) applications [1]. We extend prior literature on indoor photovoltaic energy harvesting by fabricating and demonstrating a wireless sensor node in which a spectrum-tailored organic solar cell is used to charge a supercapacitor, which in turn intelligently powers a radio payload using a state-based control strategy.

1.1. Application Environment

Because solar cells are generally optimized for outdoor use, their performance is traditionally measured under 1-sun standard irradiance of 100 mW/cm^2 with AM 1.5G spectrum. However, indoor conditions differ considerably from this conventional scenario. First, indoor light intensity is characterized in illuminance, as seen by the human eye. Standard indoor illumination at 300 lux corresponds to 100-500 $\mu W/cm^2$ irradiance depending on the light source. Second, the light spectrum is very different than the sun. The absorption spectrum of organic photo-active materials is well-suited to absorb indoor light spectra, so they are a natural solution for indoor light harvesting. Figure 1 illustrates that the solar cell's absorption spectra overlaps well with high fractions of LED and CFL emission spectra. By tailoring the energy harvester to the intended environment, we are able to operate in very low power-availability environments.

Indoor lighting intensity in workspaces and industrial settings is internationally regulated and must be above a minimum threshold [2, 3]. This lighting level is adequate to power our WSN with a periodicity below one minute, a frequency applicable for intermittent sensing applications like environmental monitoring.

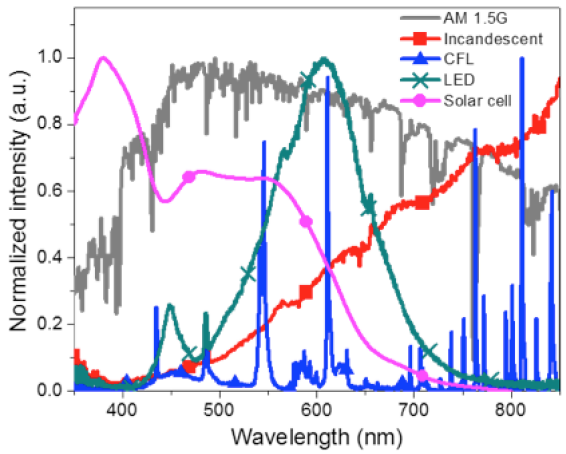

Figure 1. Absorption spectrum of the solar cell (pink), and normalized emission spectra of AM1.5G, incandescent, compact fluorescent, and LED sources.

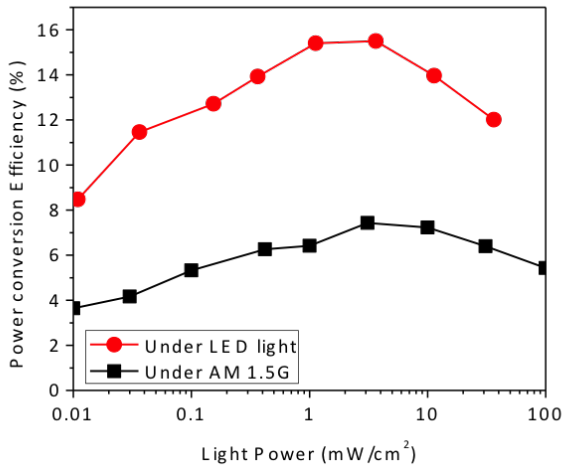

Figure 2. Evolution of PCE for the solar cell under LED and AM 1.5G sources.

2. Our System

2.1. Organic Solar Cells

Organic solar cells (OSC) currently achieve more than 10% power conversion efficiency (PCE) under 1-sun conditions [1, 2] and can be stable over several years [3, 4]. The materials involved in their fabrication can be completely printed on flexible substrates, allowing the use of large- area, high-throughput, low-cost manufacturing processes such as roll-to-roll printing. Here, OSCs based on the blend of poly[N-9'-heptadecanyl-2,7-carbazole-alt-5,5-(4,7-di-2-thienyl-2',1',3'-benzothiadiazole] (PCDTBT) and [6,6]-phenyl-C71-butyric acid methyl ester (PC71BM) (1:3.7 in ortho-dichlorobenzene with 5% dimethyl sulfoxide) are chosen. The architecture of the cell is shown in figure 3 and the fabrication followed the procedure described in [4]. We leverage spectrum-tailored OSCs to make the best use of indoor ambient energy, and are able to continuously harvest 20 $\mu W/cm^2$ [4].

For a given light source, the light power (P_{min}) at which a solar cell will stop performing well can be linked to its short circuit current (J_{sc}) under $P_{100} = 100\ mW/cm^2$ by: $J_{dark}/J_{sc} \approx P_{min}/P_{100}$. In order to optimize OSCs for indoor light, it is critical to maintain their dark current as low as possible. Control of the dark current can be achieved by varying the thickness of the top polyethylenimine ethoxylated (PEIE) layer. Figure 2 shows the evolution of the PCE of PCDTBT:PC71BM solar cell under an AM1.5G light source and a standard LED light source for varying light intensities. The cells have a dark current of 2 $\mu A/cm^2$ at a bias of -0.5 *volts*, while their J_{sc} under 1-sun is 12 mA/cm^2. As a result, they achieve more than 4% of power conversion efficiency under 10 $\mu W/cm^2$ of AM 1.5G light, from 5.4% under 100 $\mu W/cm^2$. Moreover, because of the adequacy of the absorption spectrum of PCDTBT:PC71BM, those solar cells under an LED light source demonstrate PCEs between 7% and 15%. Figure 4 shows the typical J-V curve of the PCDTBT based solar cells under typical indoor conditions: 340 *lux* of either AM1.5G light (corresponding to 310 $\mu W/cm^2$) and LED light (corresponding to 124 $\mu W/cm^2$ of power). The maximum power produced by this cell is 15.75 $\mu W/cm^2$ under LED light and 19.6 $\mu W/cm^2$ under AM 1.5G. Despite the almost three-fold difference in light power, the solar cell provides similar amounts of power under them.

2.2. Supercapacitor

To meet these power demands, energy harvested from the OSC accumulates in the high-power energy reservoir of a printed carbon supercapacitor [5, 6] for use during radio transmission. Figure 5 shows our reservoir is able to supply 9.8 mW/cm^2 of reservoir footprint, and therefore

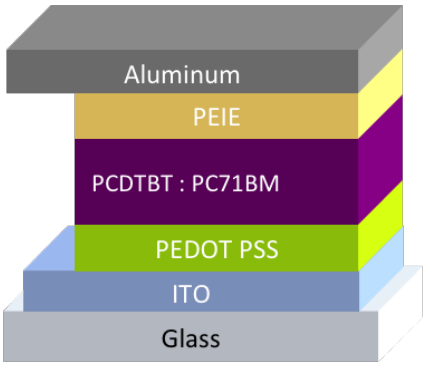

Figure 3. Architecture of the solar cell considered.

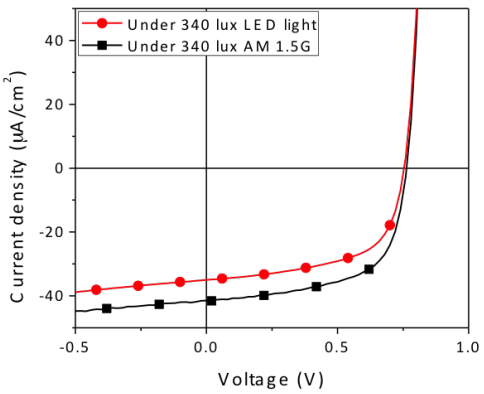

Figure 4. J-V curve of a solar cell under 340 lux from LED and AM1.5G source.

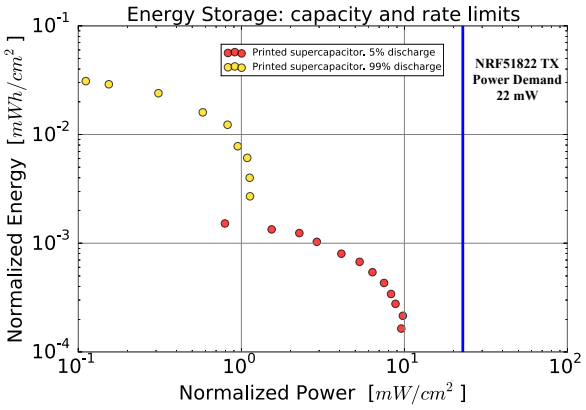

Figure 5. Ragone plot: power capabilities of printed supercapacitor. NRF51822 max power requirement is blue vertical line.

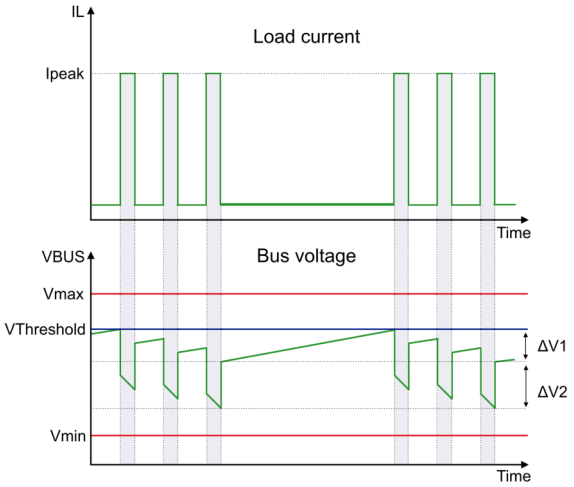

Figure 6. Acquisition and transmission is triggered once the threshold voltage is reached

a minimum supercapacitor footprint of 2.2 cm^2 is necessary to meet the radio power demands. It is important to avoid oversizing the supercapacitor in this low-power harvesting environment to mitigate leakage currents. An excessively leaky reservoir can quickly make the WSN inoperable in low-power harvesting environments. We leverage printed supercapacitor manufacturing because it enables the energy storage parameters to be tailored by controlling footprint geometry, layer thickness, and parallel or series inter-cell connections.

2.3. Radio and Sensor

We selected Nordic Semiconductors Bluetooth low energy radio NRF51822 for its low peak-power demands. This 2.4 gigahertz transceiver is seen transmitting 56 packets in figure 7 while drawing 6.9 mA peak current at 3.2 $volts$. The peak power of these transmissions is therefore 22 mW, nearly 1000 times the available power from the OSC. The radios sleep current is 3 μA. Additionally, we avoid energy-costly handshaking protocols by transmitting data using advertising packets.

NRF51822 can operate at voltages from 1.8 to 3.6 $volts$. To measure accelerations, we used the low power 10 bit accelerometer ADXL345 from Analog Devices sensing at 200 Hz with 145 μA current consumption. By leveraging these low operating and sleep currents, were able to best mitigate the costs of performing our sensing and transmission protocols.

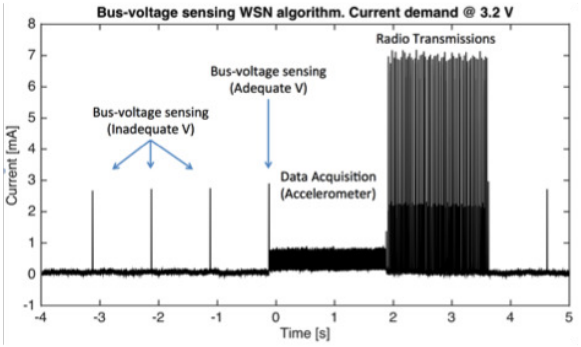

Figure 7. Voltage-dependent triggering protocol. Sensing and transmission only occurs when bus-voltage threshold is reached.

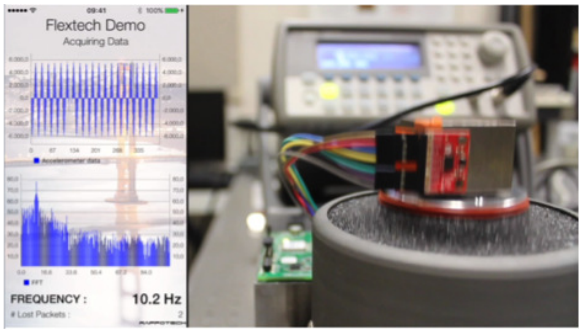

Figure 8. Frequency processing of data acquired from sensor mounted on voice coil oscillating at 10.2 Hz.

2.4. Triggering Algorithm

We implement a triggering algorithm wherein the WSN lies dormant until the energy stored in the supercapacitor is adequate to power sensing and transmission protocols. The WSN cold-starts when the radio's low voltage bound is reached at 1.8 *volts* and immediately enters a sleep state. The supply voltage continues to scale linearly as the supercapacitor accumulates charge. The WSN wakes periodically to measure the reservoir's bus voltage (V_{bus}). Once (V_{bus}) exceeds a threshold voltage, the WSN senses from the accelerometer and transmits via advertising packet. The triggering voltage must be above the cold start voltage plus the worst case voltage drop $\Delta V1 + \Delta V2$ seen in figure 6.

In our tests, the coulombic cost of acquisition and transmission are calculated to be 2.2 mC. This provides a $\Delta V1$ voltage drop of 55 mV for a supercapacitance of 40 mF. Our peak current of 6.9 mA produces a $\Delta V2$ ohmic drop of 280 mV. These voltage drops sum to 335 mV. To provide an adequate safety factor for our demonstration, we set the triggering voltage to 2.3 *volts*, 500 mV above our cold-start voltage.

3. Demonstration and Conclusion

We show a functional WSN in figure 8 that integrates a printable organic solar cell and printed supercapacitor to power the WSN in indoor light. Power is managed with a simple voltage-based triggering algorithm that only enables data acquisitions and transmission once the supercapacitor is adequately charged. This demonstration shows time-series acceleration data being transmitted to a base station where it is processed to view the frequency response.

3.1. Conclusion

With this work we demonstrate a wireless sensor node capable of running exclusively on indoor light, illustrating feasibility for nodes that can operate autonomously in low-light and indoor environments.

References

[1] Tuukkanen S, Välimäki M, Lehtimäki S, Vuorinen T and Lupo D 2016 *Nature Publishing Group* 1–9
[2] DiLaura D *et al.* 2011 *Illuminating Engineering Society of North America* **120**
[3] EN12464-1 *European Standard*
[4] Lechêne B P *et al.* 2016 *Nano Energy* **26** 631–640
[5] Cowell M *et al.* 2014 *Journal of Physics: Conference Series* **557** 012061–5
[6] Kötz R and Carlen M 2000 *Electrochimica Acta* **45** 2483–2498